How to cite: Angew. Chem. Int. Ed. 2024, e202420249
doi.org/10.1002/anie.202420249

Anti-Perovskite Hot Paper

Chiral Metal-Free Anti-Perovskite with Strong Chiroptical Nonlinearity

Zhaoyu Wang[+], Xin Qiu[+], Hebin Wang[+], Wenkai Zhao, Sehrish Gull, Haolin Lu, Zechen Hao, Bing Sun, Xin Zeng, Xinfeng Liu, Hao-Li Zhang, Yongsheng Chen, Tingchao He, and Guankui Long**

Abstract: The nonlinear chiroptical properties of chiral metal halide perovskite has attracted substantial attention in recent years. In order to overcome the inherent limitations of metal halide, such as high costs, potential toxicity, challenges with recycling, especially the limited laser-induced damage threshold (LDT), we have successfully constructed the first chiral metal-free anti-perovskite, with the aim of utilizing it in second harmonic generation-circular dichroism (SHG-CD). Moreover, the anti-perovskite composed entirely of small organic ions typically display a more extensive transparent window, which could contribute a high LDT. Herein two chiral metal-free anti-perovskites, *R*/*S*-MCN [(*R*/*S*-MBA)$_6$Cl(NH$_4$Cl$_6$)] were constructed, and exhibit strong second-harmonic generation response from 800 to 980 nm. The second-order nonlinear optical coefficient of the chiral metal-free anti-perovskite reaches 0.89 pm/V, which is higher than that of commercial Y-cut quartz. Most importantly, both *R*- and *S*-MCN exhibit a large nonlinear optical activity with a high SHG dissymmetry factor ($g_{SHG\text{-}CD}$) of 0.60 and a high laser-induced damage threshold of 71 mJ/cm^2, which is higher than that of most reported chiral perovskites. Our findings indicate that chiral metal-free anti-perovskite have the potential to be a valuable addition to the development of next-generation nonlinear chiroptical devices.

Second-harmonic generation (SHG) crystals could double the frequency of incident lasers,[1] which are pivotal in modern laser science,[2] technology and quantum optics.[3] If the SHG crystals have chirality simultaneously, the SHG response will be different under the left-handed and right-handed circularly polarized light excitation, which is called second-harmonic generation circular dichroism (SHG-CD).[4] Therefore, the polarization of light can be controlled in the nonlinear optical (NLO) regime and the analysis of the chirality of materials or the detection of the handedness of CP lights can be achieved by SHG-CD. The intriguing chiral NLO response has attract considerable interest due to it has many crucial applications, such as optical encryption and security, nonlinear holographic imaging and quantum information processing.[5]

Chiral perovskites are desirable materials for both SHG and SHG-CD due to their intrinsic non-centrosymmetric chiral structure.[6] Opposite from the conventional perovskites composed by A, B-site cation and X-site anion, anti-perovskites are constructed by A, B-site anion and X-site cation. Recently, several anti-perovskites were reported, and showed many remarkable properties, such as strong SHG response, large ferroelectric polarization, and ultralow dose X-ray detection.[7] However, among them, (*R*/*S*-3-chloroquinuclidinium)$_3$(CdCl$_3$)(CdCl$_4$) is the only reported chiral anti-perovskite which involve toxic heavy metal (Cd). Thus, we focused on the chiral metal-free anti-perovskite in this work, which embrace the advantages of organic semi-

[*] Z. Wang,[+] H. Wang,[+] W. Zhao, S. Gull, H. Lu, Z. Hao, X. Zeng, Prof. G. Long
School of Materials Science and Engineering, Tianjin Key Lab for Rare Earth Materials and Applications, Smart Sensing Interdisciplinary Science Center, Renewable Energy Conversion and Storage Center (RECAST), National Institute for Advanced Materials, Nankai University
Tianjin 300350, China
E-mail: longgk09@nankai.edu.cn

X. Qiu,[+] Prof. T. He
Key Laboratory of Optoelectronic Devices and Systems of Ministry of Education and Guangdong Province, College of Physics and Optoelectronic Engineering, Shenzhen University
Shenzhen 518060, China
E-mail: tche@szu.edu.cn

B. Sun, H.-L. Zhang
State Key Laboratory of Applied Organic Chemistry (SKLAOC), Key Laboratory of Special Function Materials and Structure Design (MOE), College of Chemistry and Chemical Engineering, Lanzhou University
Lanzhou 730000, China

X. Zeng, Prof. X. Liu
CAS Key Laboratory of Standardization and Measurement for Nanotechnology, National Center for Nanoscience and Technology
Beijing 100190, China

Prof. Y. Chen
The Centre of Nanoscale Science and Technology and Key Laboratory of Functional Polymer Materials, Institute of Polymer Chemistry, Renewable Energy Conversion and Storage Center (RECAST), College of Chemistry, Nankai University
Tianjin 300071, China

[+] These authors contributed equally to this work.

conductors, such as eco-friendly synthesis, low cost, lightweight, structural tunability and mechanical flexibility.[8] In principle, chiral anti-perovskites should also exhibit the superior optical, electrical and spintronic properties as chiral perovskites, including chirality, non-centrosymmetric structure, compositional tunability, structural diversity, and tunable absorption and emission, which make them attractive for SHG-CD. In particular, chiral perovskites usually show undesirable laser-induced damage threshold (LDT) due to high light absorption coefficient.[9] Intriguingly, the chiral metal-free anti-perovskites are composed of small organic ions typically display an outstanding optical transparency, which could increase the LDT. However, the chiral NLO properties of chiral anti-perovskites still remain unexplored.

In this work, we designed and synthesized the first chiral metal-free anti-perovskites, (*R*/*S*-MBA)$_6$Cl(NH$_4$Cl$_6$) (*R*/*S*-MCN, MBA = α-methylbenzylammonium) and systematically investigated their nonlinear chiroptical properties. As shown in the Figure 1, the A-, B-, and X-sites of *R*/*S*-MCN are $[NH_4Cl_6]^{5-}$, Cl^-, MBA^+, respectively. These chiral metal-free anti-perovskites exhibit broadband SHG response from 800 to 980 nm, and the second-order NLO coefficient of *S*-MCN reaches 0.89 pm/V. Moreover, the chiral SHG dissymmetry factor $g_{SHG\text{-}CD}$ of *S*-MCN reaches 0.60, which is higher than that of the reported lead-free metal halides. Most importantly, owing to the excellent optical transparency of these chiral metal-free anti-perovskites, a high laser-induced damage threshold of 71 mJ/cm^2 is obtained, which is larger than that of most chiral perovskites and thus favorable for practical application. We expect that our findings would shed light on the exploration of novel chiral metal-free anti-perovskite for future engineering of nonlinear chiroptics and other functionalities.

The chiral metal-free anti-perovskites were obtained by slow evaporation method at room temperature, and their single crystal structures were determined through the single crystal X-ray diffraction at 100 K. The phase purity of the as-grown crystals was confirmed by the Rietveld refinement of the powder X-ray diffraction pattern against the crystal structure determined at 100 K (Figure S1 and S2). Both *R*- and *S*-MCN crystallized in the *R*3 *Sohncke* space group with lattice constants of $a = 25.5474(2)$ Å, $b = 25.5474(2)$ Å, $c = 7.36090(10)$ Å, and $a = 25.5808(3)$ Å, $b = 25.5808(3)$ Å, $c = 7.33170(10)$ Å, $\alpha = \beta = 90°$, $\gamma = 120°$, respectively (Table S1).[10] While *rac*-MCN crystallized into the $R\bar{3}$ centrosymmetric space group with lattice constants of $a = 25.796(4)$ Å, $b = 25.796(4)$ Å, $c = 7.000(2)$ Å (Table S1).[10] As expected, it consists of the surrounding MBA^+ cations, Cl^- is in the center, and $[NH_4Cl_6]^{5-}$ anions surrounded by the octahedra and the *R*-MBA^+ is arranged in a clockwise spiral stack, while the *S*-MBA^+ is arranged in a counter-clockwise spiral stack. As shown in Figure 2, the $[(MBA)_6Cl]^{5+}$ octahedral structure formed by MBA^+ and Cl^- is separated by $[NH_4Cl_6]^{5-}$. There are no direct connections between octahedra with the chiral MBA^+ as vertexes due to the steric hindrance, forming a 0D chiral metal-free anti-perovskite structure. The corresponding enantiomorphic nature is further verified by the vibrational circular dichroism (VCD) spectra (Figure S3).[11] The VCD peaks around 900 to 1000 cm^{-1} correspond to the bending vibration of C–H bond in MBA. As expected, the infrared spectra of both enantiomorphic crystals are almost the same, whereas the corresponding VCD spectra are nearly mirror symmetric. Additionally, to further confirm the chirality of our chiral anti-perovskites, the CD measurement was carried out. *R*- and *S*-MCN also exhibit a mirror symmetric CD signal as shown in Figure S4. As expected, no CD signal was observed for *rac*-MCN. Their thermal stability was investigated by using the thermogravimetric analysis (TGA), which revealed the decomposition temperature of *R*/*S*-MCN is above 195 °C (Figure S5). The structural stability of *R*/*S*-MCN is determined by its intermolecular interactions.[9a] To deeply understand the intermolecular interactions of these chiral metal-free anti-perovskites, Hirshfeld analysis was conducted, and found that *R*-MCN and *S*-MCN exhibit similar intermolecular interactions. As shown in Figure S6 and S7, there are several deep red circular areas on the 3D d_{norm} surface which represents the N–H···Cl interaction. According to the 2D-fingerprint plots, *R*-MCN and *S*-MCN

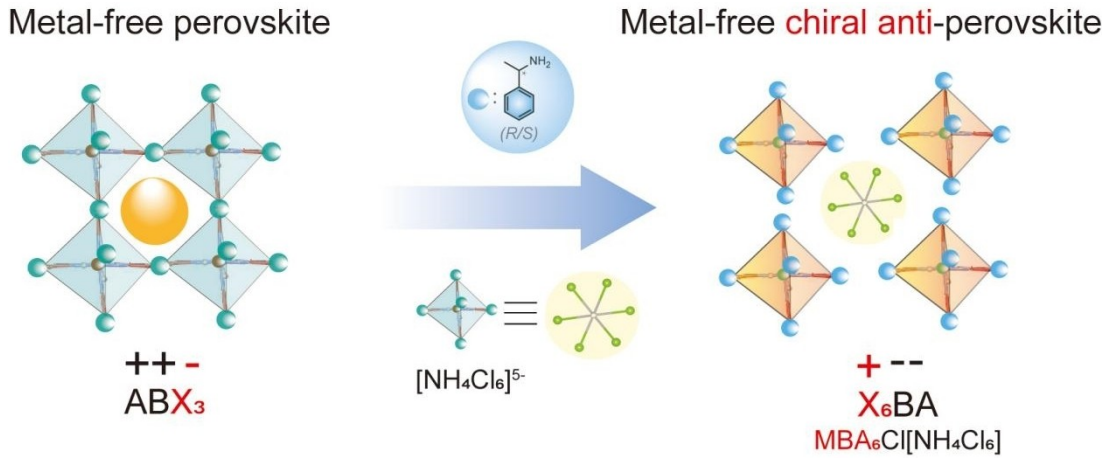

Figure 1. The schematic diagram of constructing the chiral metal-free anti-perovskite.

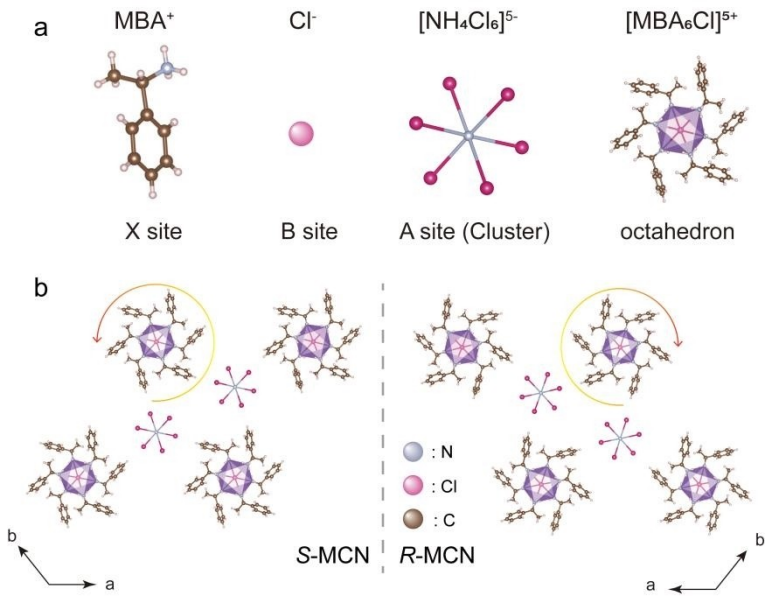

Figure 2. (a) The composition of *R*/*S*-MCN; (b) The packing view of *R*-MCN (right) and *S*-MCN (left).

exhibit a more pronounced N–H···Cl interaction (21.0 % for *R*-MCN and *S*-MCN) than N–H···N interaction (2.1 % for *R*-MCN and 2.2 % for *S*-MCN) which further confirms the formation of $[MBA_6Cl]^{5+}$ octahedra.

The distortion of the coordinated polyhedral could also influence the linear and nonlinear optical properties of the anti-perovskite.[12] Due to the chiral induction effect by the *R*/*S*-MBA cations, the $[MBA_6Cl]^{5+}$ octahedrons in *R*/*S*-MCN are more distorted. Similar phenomenon has been widely observed in chiral metal halides. Equation 1 is employed to quantify the bond length distortion index (D) of $[(MBA)_6Cl]^{5+}$,[12b,13]

$$D = \frac{1}{6}\sum_{i=1}^{6}\frac{|d_i - d_0|}{d_0} \quad (1)$$

where d_i represents the length of the N–Cl bond and d_0 is the averaged N–Cl bond length. The calculated D is 3.01×10^{-3} and 1.49×10^{-3} for *S*-MCN and *R*-MCN, respectively, which is comparable to that of the reported chiral perovskites with strong SHG response.[14]

Subsequently, the photophysical properties of the chiral metal-free anti-perovskites were investigated. The UV/Vis-IR absorption spectra of *R*/*S*-MCN depicts an exceptional optical transparency (~90 %) without absorption in a very wide spectral range from 300 to 1000 nm (Figure 3a). Such a broad transparency range indicates that it could be effectively pumped by lasers with high laser power. We also measured the absorption spectrum of *rac*-MCN, which exhibit similar absorption band with *R*/*S*-MCN (Figure S8). To further understand the electronic properties, their electronic band structures were calculated based on density functional theory (DFT). As shown in Figure 3b, the band structures exhibit fairly nondispersive character, which is attributed to the systems being composed of independent molecular units that have no covalent bonds between each other. The band gap of both *R*- and *S*-MCN is estimated to 3.78 eV (Figure S9). Meanwhile, the valence band maximum (VBM) is mainly contributed by Cl-2*p* orbitals, while the conduction band minimum (CBM) is mainly composed of the C-2*p* orbitals (Figure S10). Subsequently, the luminescent properties of the anti-perovskite were characterized. As shown in Figure 3c, both *R*- and *S*-MCN exhibit a typical two-band emission ($\lambda_{ex}=265$ nm), one in the ultraviolet region and the other in the visible region with three major peaks around 400, 430 and 460 nm. The emission peak around 290 nm was identified as fluorescent emission (Figure 3c), with a short lifetime of 19.09 ns (Figure S11). The luminescent peaks at 400, 430 and 460 nm are assigned to the 0–0, 0–1, and 0–2 transitions caused by different vibrational modes. They exhibit afterglow property with a much longer lifetime of 55.61 ms at 100 K and its intensity increases with the decreasing of temperature without peak shift, which should be assigned as the phosphorescent emission (Figure 3d and Figure S12).[15] To identify the phosphorescence contribution of our chiral anti-perovskite, the emission spectra of their corresponding organic ionic crystals (*R*/*S*-MBACl) were also measured. As shown in Figure S13, MBACl also shows an emission band from 400 to 600 nm at 100 K which is similar with *R*/*S*-MCN. Therefore, the phosphorescence of *R*/*S*-MCN should be originally derived from its aromatic MBA ring.

Owing to the non-centrosymmetric crystal structures of *R*- and *S*-MCN, the second-order optical nonlinearity is expected. As shown in Figure 4a, a home-built micro-area NLO characterization system was employed to investigate the SHG properties of the chiral metal-free anti-perovskites in the reflection geometry (refer the Experimental Section). Both *R*- and *S*-MCN exhibit a strong SHG

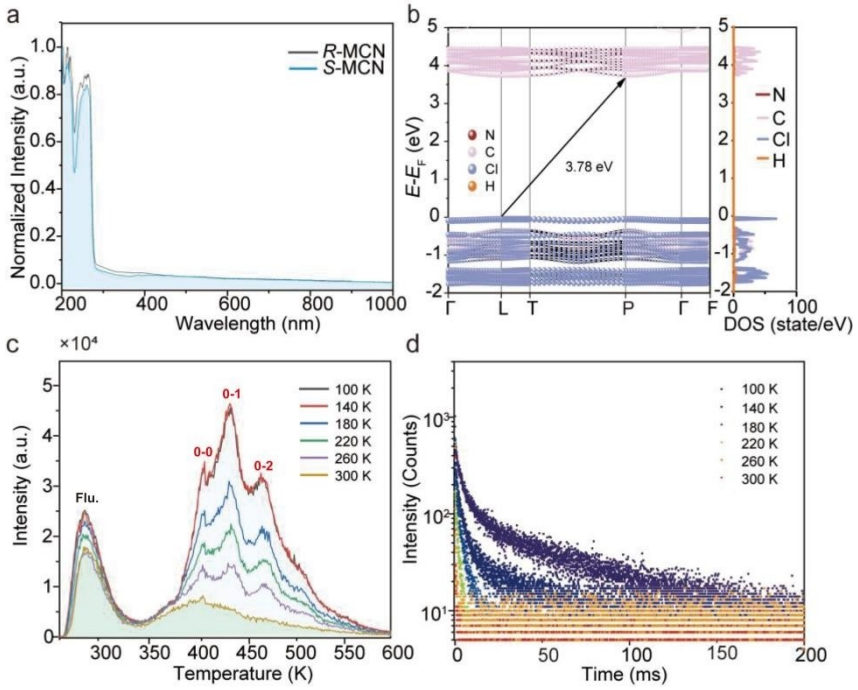

Figure 3. (a) The absorption spectrum of *R*/*S*-MCN. (b) The calculated band structure and density of states of *R*-MCN. (c) The temperature-dependent photoluminescence spectra of *R*-MCN. (d) The temperature-dependent time-resolved photoluminescence spectra of *R*-MCN.

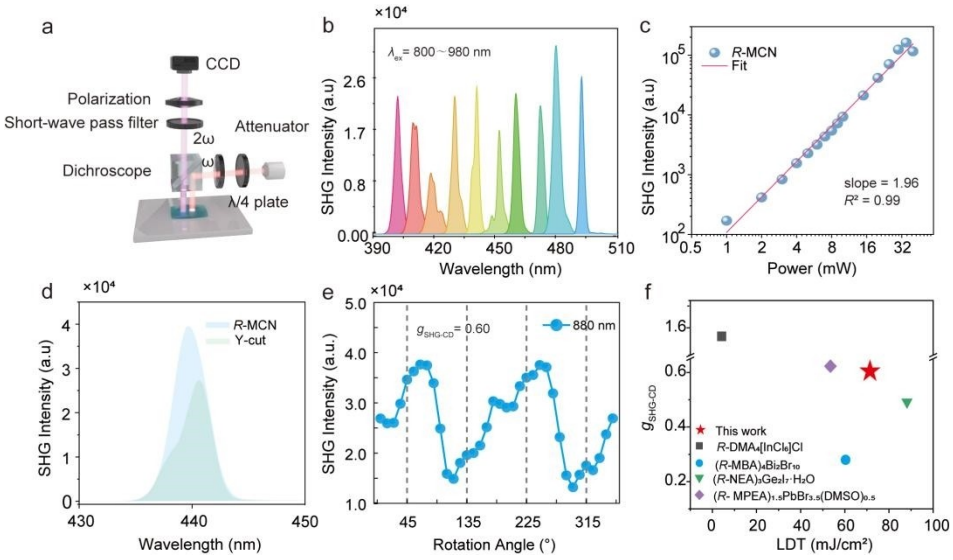

Figure 4. (a) Schematic of the home-built micro-area NLO characterization system. (b) The SHG intensity of the *R*-MCN crystal pumped at various wavelengths. (c) Logarithmic diagrams of the power-dependent SHG intensity. The solid line is the linear fitting with a slope of 1.96. (d) Comparison of the SHG signals of *R*-MCN and commercial Y-cut quartz under the same experimental conditions. (e) The SHG-CD intensity as a function of the rotation angle of the λ/4 plate. The excitation and detection wavelengths are 880 and 440 nm, respectively. (f) The comparison of $g_{SHG\text{-}CD}$ and LDT in literatures and this work.

response under a wide excitation wavelength from 800 to 980 nm (as shown Figure 4b). During the SHG measurement, the same experimental condition was used. To quantify the second-order NLO coefficient (d_{eff}), Y-cut quartz was utilized as a reference. As a result, the d_{eff} of *R*-MCN and *S*-MCN at 880 nm were roughly estimated to be ~0.86 and ~0.89 pm/V, respectively (Figure 4c). It should be noted that the d_{eff} of our chiral metal-free anti-perovskites are much larger than that of the commercial SHG crystal (1.4×Y-cut quartz for *R*-MCN and 1.5×Y-cut quartz for *S*-MCN) and many chiral perovskites, such as (R-1-(1-naphthyl)ethylammonium)$_2$CuCl$_4$ (0.13 pm/V), (R/S-3-aminopiperidine)$_4$AgBiBr$_{12}$ (0.28 pm/V) and (R-1-(1-naphthyl)ethylammonium)$_3$Ge$_2$I$_7$·H$_2$O (0.65 pm/V) (Fig-

ure S14). Additionally, the SHG intensity showed a quadratic dependence on the power of the pumped laser (as shown in Figure 4d), consistent with the two-photon nature of the SHG process. The SHG intensity dropped when the excitation power was larger than 32 mW, indicating a high laser-induced damage threshold (LDT) of 71 mJ/cm^2. Such a high LDT should be attributed to the larger band gap of the chiral anti-perovskites, which is larger than that of many chiral perovskites and is favorable for practical applications.[16] Thus, the development of chiral metal-free anti-perovskite open up a new avenue to develop high performance nonlinear optical material towards real applications.

The SHG-CD of *R*- and *S*-MCN were subsequently investigated.[17] During the measurement, the excitation laser was switched between left- and right-handed circularly polarization (LCP and RCP) states by using a polarizer and a λ/4 wave plate. Typically, as shown in Figure 4e and Figure S14, under 880 nm laser excitation, the SHG intensity of *R*/*S*-MCN varies as the rotation of the λ/4 plate change. *R*-MCN exhibits an obviously stronger SHG intensity under the LCP light pumping than that under the RCP light pumping, which is attributed to the nonlinear chiroptical effect. The dissymmetry factor of SHG-CD ($g_{SHG\text{-}CD}$) is calculated based on Equation 2,

$$g_{SHG-CD} = \frac{2(I_{LCP} - I_{RCP})}{(I_{LCP} + I_{RCP})} \quad (2)$$

Where I_{LCP} and I_{RCP} represent the SHG intensities under LCP and RCP light excitation, respectively.[18] Interestingly, the $g_{SHG\text{-}CD}$ of our chiral metal-free anti-perovskites can reach 0.60 for *R*-MCN and −0.37 for *S*-MCN (Figure S15), which are larger than most of the chiral perovskites as shown in Figure 4f and Table S2.[19]

Conclusion

The first chiral metal-free anti-perovskites, *R*/*S*-MCN [(*R*/*S*-MBA)$_6$Cl(NH$_4$Cl$_6$)] were successfully designed and constructed. Both *R*-MCN and *S*-MCN crystallize in non-centrosymmetric *Sohncke* space group, *R*3, with a broad transparent region (300–1000 nm) and exhibit strong SHG response. The second-order NLO coefficient of *R*-MCN and *S*-MCN reaches ~0.86 and ~0.89 pm/V, respectively. Surprisingly, owing to the outstanding optical transparency of *R*-MCN and *S*-MCN, they exhibit a high LDT of 71 mJ/cm^2, which is larger than that of most chiral perovskites. More importantly, *R*-MCN and *S*-MCN possess strong SHG-CD effect over a wide range of wavelengths, with $g_{SHG\text{-}CD}$ up to 0.60 under 880 nm excitation, which is higher than that of most chiral lead-free perovskites. Our work develops a novel family member of chiral semiconductor, chiral metal-free anti-perovskites, which combines the advantages of organic semiconductors and perovskite with chirality. Our work will stimulate the research to develop novel nonlinear chiroptical material with both high LDT and excellent performance.

Acknowledgements

The authors gratefully acknowledge the financial support from the National Natural Science Foundation of China (92256202, 52473305, U22A20399, 12261131500, 52103218, 62475169), the Fundamental Research Funds for the Central Universities, Nankai University (Grant Number: 023–63233038) and the 111 Project (B18030).

Conflict of Interest

The authors declare no conflict of interest.

Data Availability Statement

The data that support the findings of this study are available from the corresponding author upon reasonable request.

Keywords: Chiral Anti-Perovskite · Metal-Free Material · Second-Harmonic Generation · Laser-Induced Damage Threshold · Nonlinear Chiroptics

[1] a) X. Han, P. Cheng, R. Shi, Y. Zheng, S. Qi, J. Xu, X.-H. Bu, *Mater. Horiz.* **2023**, *10*, 1005–1011; b) S. Jiang, P. Zhao, G. Xing, H. Kang, X. Li, T. Zhao, B. Li, T. Zhang, *Adv. Opt. Mater.* **2023**, *11*, 2203078.

[2] V. Y. Sirenko, O. I. Kucheriv, E. Gumienna-Kontecka, S. Shova, I. y. A. Gural′skiy, *Dalton Trans.* **2022**, *51*, 16536–16544.

[3] a) Z. Yu, S. Cao, Y. Zhao, Y. Guo, M. Dong, Y. Fu, J. Zhao, J. Yang, L. Jiang, Y. Wu, *ACS Appl. Mater. Interfaces* **2022**, *14*, 39451–39458; b) J. Zhao, Y. Zhao, Y. Guo, X. Zhan, J. Feng, Y. Geng, M. Yuan, X. Fan, H. Gao, L. Jiang, Y. Yan, Y. Wu, *Adv. Funct. Mater.* **2021**, *31*, 2105855.

[4] a) D. Fu, J. Xin, Y. He, S. Wu, X. Zhang, X.-M. Zhang, J. Luo, *Angew. Chem. Int. Ed.* **2021**, *60*, 20021–20026; b) X. Fu, Z. Zeng, S. Jiao, X. Wang, J. Wang, Y. Jiang, W. Zheng, D. Zhang, Z. Tian, Q. Li, A. Pan, *Nano Lett.* **2023**, *23*, 606–613.

[5] a) J. Guan, Y. Zheng, P. Cheng, W. Han, X. Han, P. Wang, M. Xin, R. Shi, J. Xu, X.-H. Bu, *J. Am. Chem. Soc.* **2023**, *145*, 26833–26842; b) Z. Guo, J. Li, J. Liang, C. Wang, X. Zhu, T. He, *Nano Lett.* **2022**, *22*, 846–852.

[6] a) H. Wang, J. Li, H. Lu, S. Gull, T. Shao, Y. Zhang, T. He, Y. Chen, T. He, G. Long, *Angew. Chem. Int. Ed.* **2023**, *62*, e202309600; b) Z. Wen, R. Lu, F. Gu, K. Zheng, L. Zhang, H. Jin, Y. Chen, S. Wang, S. Pan, *Adv. Funct. Mater.* **2023**, *33*, 2212095; c) S. Ma, J. Ahn, J. Moon, *Adv. Mater.* **2021**, *33*, 2005760.

[7] a) M. Li, X. Zhang, Z. Xiong, Y. Li, Y. Zhou, X. Chen, Y. Song, M. Hong, J. Luo, S. Zhao, *Angew. Chem. Int. Ed.* **2022**, *61*, e202211151; b) L. Liu, S.-Y. Liu, Y. Shi, C.-L. Fang, S. Zhao, H.-Y. Shen, M.-X. Chen, Z.-J. Wang, Y. Ma, Y. Liu, Y. Feng, J. Tang, H.-Y. Ye, G. Niu, *Nat. Photonics* **2024**, *18*, 990–997; c) G. Long, R. Sabatini, M. I. Saidaminov, G. Lakhwani, A. Rasmita, X. Liu, E. H. Sargent, W. Gao, *Nat. Rev. Mater.* **2020**, *5*, 423–439; d) A. Pabst, *Z. Kristallogr. Cryst. Mater.* **1934**, *89*, 514–517; e) Z.-X. Wang, Y. Zhang, Y.-Y. Tang, P.-F. Li, R.-G. Xiong, *J. Am. Chem. Soc.* **2019**, *141*, 4372–4378; f) Z. Wei, W.-Q. Liao, Y.-Y. Tang, P.-F. Li, P.-P. Shi, H. Cai, R.-G. Xiong, *J. Am. Chem. Soc.* **2018**, *140*, 8110–8113; g) J.-T. Lin, D.-G. Chen, L.-S. Yang, T.-C. Lin, Y.-H. Liu, Y.-C. Chao, P.-

T. Chou, C.-W. Chiu, *Angew. Chem. Int. Ed.* **2021**, *60*, 21434–21440; h) J.-X. Gao, W.-Y. Zhang, Z.-G. Wu, Y.-X. Zheng, D.-W. Fu, *J. Am. Chem. Soc.* **2020**, *142*, 4756–4761; i) K. Kim, E. Vetter, L. Yan, C. Yang, Z. Wang, R. Sun, Y. Yang, A. H. Comstock, X. Li, J. Zhou, L. Zhang, W. You, D. Sun, J. Liu, *Nat. Mater.* **2023**, *22*, 322–328; j) M.-E. Sun, Y. Wang, F. Wang, J. Feng, L. Wang, H. Gao, G. Chen, J. Gu, Y. Fu, K. Bu, T. Fu, J. Li, X. Lü, L. Jiang, Y. Wu, S.-Q. Zang, *J. Am. Chem. Soc.* **2023**, *145*, 8908–8916; k) M. K. Jana, R. Song, Y. Xie, R. Zhao, P. C. Sercel, V. Blum, D. B. Mitzi, *Nat. Commun.* **2021**, *12*, 4982; l) J. Ma, C. Fang, C. Chen, L. Jin, J. Wang, S. Wang, J. Tang, D. Li, *ACS Nano* **2019**, *13*, 3659–3665.

[8] a) T. Sheikh, S. Maqbool, P. Mandal, A. Nag, *Angew. Chem. Int. Ed.* **2021**, *60*, 18265–18271; b) Z. Wei, W.-Q. Liao, Y.-Y. Tang, P.-F. Li, P.-P. Shi, H. Cai, R.-G. Xiong, *J. Am. Chem. Soc.* **2018**, *140*, 8110–8113; c) Z.-X. Wang, Y. Zhang, Y.-Y. Tang, P.-F. Li, R.-G. Xiong, *J. Am. Chem. Soc.* **2019**, *141*, 4372–4378; d) P.-F. Li, Y.-Y. Tang, W.-Q. Liao, P.-P. Shi, X.-N. Hua, Y. Zhang, Z. Hong, H. Cai, R.-G. Xiong, *Angew. Chem. Int. Ed.* **2018**, *57*, 11939–11942; e) H.-Y. Ye, Y.-Y. Tang, P.-F. Li, W.-Q. Liao, J.-X. Gao, X.-N. Hua, H. Cai, P.-P. Shi, Y.-M. You, R.-G. Xiong, *Science* **2018**, *361*, 151–155.

[9] a) M. Ma, X. Jiang, Z. Zang, X. Wen, W. Zhou, H. Wu, S. Peng, Y. Liu, H. Li, D. Yu, H. Liang, H. Wang, W. Zhou, Z. Su, F. Zheng, X. Gao, A. V. Emeline, C. C. Stoumpos, Z. Ning, *Adv. Funct. Mater.* **2024**, *34*, 2407095; b) Y.-L. Zeng, X.-Q. Huang, C.-R. Huang, H. Zhang, F. Wang, Z.-X. Wang, *Angew. Chem. Int. Ed.* **2021**, *60*, 10730–10735.

[10] Deposition numbers 2390200 (for (*R*-MCN)), 2390199 (for (*S*-MCN)), 2404026 (for (*rac*-MCN)) and 2390199 (for (*S*-MCN)) (298 K) contain the supplementary crystallographic data for this paper. These data are provided free of charge by the joint Cambridge Crystallographic Data Centre and Fachinformationszentrum Karlsruhe Access Structures.

[11] a) Y. Yan, K. Deng, Z. Yu, Z. Wei, *Angew. Chem. Int. Ed.* **2009**, *48*, 2003–2006; b) X. Yan, R. Cao, R. Zhang, H. Gao, Y. Xiao, *Adv. Funct. Mater.* **2024**, *34*, 2410012.

[12] a) S. Cui, H. Wu, Z. Hu, J. Wang, Y. Wu, H. Yu, *Adv. Sci.* **2023**, *10*, 2204755; b) Y. Liu, Y.-P. Gong, S. Geng, M.-L. Feng, D. Manidaki, Z. Deng, C. C. Stoumpos, P. Canepa, Z. Xiao, W.-X. Zhang, L. Mao, *Angew. Chem. Int. Ed.* **2022**, *61*, e202208875.

[13] a) D. Appleby, P. B. Hitchcock, K. R. Seddon, J. E. Turp, J. A. Zora, C. L. Hussey, J. R. Sanders, T. A. Ryan, *J. Chem. Soc. Dalton Trans.* **1990**, 1879–1887; b) V. T. Coombe, G. A. Heath, T. A. Stephenson, D. K. Vattis, *J. Chem. Soc. Dalton Trans.* **1983**, 2307–2309; c) C. Wang, T. Song, P. Yan, S. Hu, C. Xiang, Z. Wu, H. Li, H. Zhao, L. Han, C. Sheng, *eScience* **2023**, *3*, 100185; d) Z. Zhang, W. Liang, J. Xue, X. Li, K. Wu, H. Lu, *ACS Nano* **2024**, *18*, 5890–5897; e) Q. Wang, H. Zhu, Y. Tan, J. Hao, T. Ye, H. Tang, Z. Wang, J. Ma, J. Sun, T. Zhang, F. Zheng, W. Zhang, H. W. Choi, W. C. H. Choy, D. Wu, X. W. Sun, K. Wang, *Adv. Mater.* **2024**, *36*, 2305604; f) M. Kim, J. Kim, J. Bang, Y. J. Jang, J. Park, D. H. Kim, *J. Mater. Chem. A* **2023**, *11*, 12876–12884; g) J. Ma, H. Wang, D. Li, *Adv. Mater.* **2021**, *33*, 2008785.

[14] a) S.-F. Yan, Y. Guo, W. Liu, S.-P. Guo, J. Wu, *Inorg. Chem.* **2024**, *63*, 73–77; b) W. Kang, X. Gao, H. Li, Y. Wei, C. Wang, Z. Tian, *Adv. Funct. Mater.* **2023**, *33*, 2300388.

[15] a) Z. An, C. Zheng, Y. Tao, R. Chen, H. Shi, T. Chen, Z. Wang, H. Li, R. Deng, X. Liu, W. Huang, *Nat. Mater.* **2015**, *14*, 685–690; b) Q. Li, Y. He, K. Lv, H. Ma, *Spectrochim. Acta Part A* **2023**, *287*, 122077.

[16] Z. Song, X. Liu, C. Yang, Q. Wu, X. Guo, G. Liu, Y. Wei, L. Meng, Y. Dang, *Adv. Opt. Mater.* **2024**, *12*, 2301272.

[17] a) A. Aghigh, S. Bancelin, M. Rivard, M. Pinsard, H. Ibrahim, F. Légaré, *Biophys. Rev. Lett.* **2023**, *15*, 43–70; b) D. Okada, F. Araoka, *Angew. Chem. Int. Ed.* **2024**, *63*, e202402081; c) Z. Li, C. Ji, Y. Fan, T. Zhu, S. You, J. Wu, R. Li, Z. Zhu, P. Yu, X. Kuang, J. Luo, *J. Am. Chem. Soc.* **2023**, *46*, 25134.

[18] J. Wang, J. Butet, A.-L. Baudrion, A. Horrer, G. Lévêque, O. J. F. Martin, A. J. Meixner, M. Fleischer, P.-M. Adam, A. Horneber, D. Zhang, *J. Phys. Chem. C* **2016**, *120*, 17699–17710.

[19] J. Lin, J. Zhou, Z. Wang, L. Li, M. Li, J. Xu, S. Wu, P. Naumov, J. Gong, *Angew. Chem. Int. Ed.* **2024**, *63*, e202416856.

Manuscript received: October 19, 2024
Accepted manuscript online: December 13, 2024
Version of record online: ■■, ■■

Communication

Anti-Perovskite

Z. Wang, X. Qiu, H. Wang, W. Zhao, S. Gull, H. Lu, Z. Hao, B. Sun, X. Zeng, X. Liu, H.-L. Zhang, Y. Chen, T. He,*
G. Long* _____ **e202420249**

Chiral Metal-Free Anti-Perovskite with Strong Chiroptical Nonlinearity

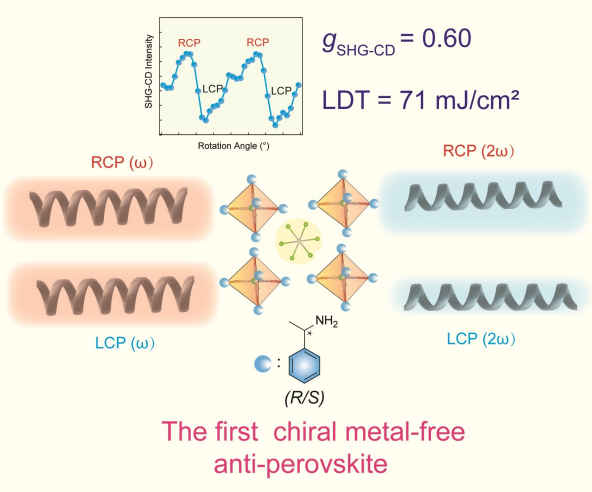

The first chiral metal-free anti-perovskite is constructed, which exhibits strong nonlinear chiroptical property. The second-harmonic generation circular dichroism of the chiral metal-free anti-perovskite reaches 0.60. Moreover, owing to the outstanding optical transparency of *R*-MCN and *S*-MCN, they exhibit a high LDT of 71 mJ/cm^2, which is larger than that of most chiral perovskites.